Chinese Physics B

Graphene metasurface-based switchable terahertz half-/quarter-wave plate with a broad bandwidth

To cite this article before publication: Xiaoqing Luo *et al* 2022 *Chinese Phys. B* in press https://doi.org/10.1088/1674-1056/ac80a8

Graphene metasurface-based switchable terahertz half-/quarter-wave plate with a broad bandwidth*

Xiaoqing Luo (罗小青)[1], Juan Luo (罗娟)[1,2], Fangrong Hu(胡放荣)[2], and Guangyuan Li(李光元)[1†]

[1]*Shenzhen Institute of Advanced Technology, Chinese Academy of Sciences, Shenzhen 518055, China*
[2]*Guilin University of Electronic Technology, Guilin 541004, China*

Metasurfaces incorporating graphene hold great promise for active manipulation of terahertz waves. However, it remains challenging to design a broadband graphene-based terahertz metasurface with switchable functionality of half-wave plate (HWP) and quarter-wave plate (QWP). Here, we propose a graphene-metal hybrid metasurface for achieving broadband switchable HWP/QWP in the terahertz regime. Simulation results show that, by varying the Fermi energy of graphene from 0 eV to 1 eV, the function of the reflective metasurface can be switched from an HWP with polarization conversion ratio exceeding 97% over a wide band ranging from 0.7 THz to 1.3 THz, to a QWP with ellipticity above 0.92 over 0.78-1.33 THz. The sharing bandwidth reaches up to 0.52 THz and the relative bandwidth is as high as 50%. We expect this broadband and dynamically switchable terahertz HWP/QWP will find applications in terahertz sensing, imaging, and telecommunications.

Keywords: Terahertz metasurface; waveplate; graphene; reconfigurable

PACS: 78.67.Pt, 42.25.Ja, 78.67.Wj

1. Introduction

Metamaterials and metasurfaces have recently emerged as promising platforms for manipulating the polarization state of electromagnetic waves because of their compactness, flexibility, and easy integration[1-6]. Half-wave plates (HWPs) and quarter-wave plates (QWPs) are two key devices for realizing polarization conversion among two orthogonal polarization states, and the left- and right-handed circular polarization (LCP and RCP) states. In the terahertz regime[7], metamaterial- or metasurface-based HWPs/QWPs are of particular interest because conventional approaches based on birefringence or total internal reflection effects are usually bulky, narrowband, and sometimes lossy.

Over the years, metamaterial-based terahertz polarization converters have evolved from narrow-band[8,9] to broadband[10-15]. However, the functionalities of these devices, which are made of metals or dielectrics, cannot be dynamically tuned. Recently, actively switchable HWPs/QWPs based on metamaterials or metasurfaces incorporating tunable materials, such as liquid crystals, vanadium dioxide (VO_2, or

* Project supported by Shenzhen Research Foundation (JCYJ20180507182444250).
† Corresponding author. E-mail: gy.li@siat.ac.cn

graphene, have attracted increasing attentions. Based on metamaterials incorporating liquid crystals, Vasić [16] and Ji *et al.*[17] respectively proposed electrically tunable terahertz polarization converters, of which the bandwidths are only 0.056 THz and 0.35 THz, respectively. Based on VO_2-metal metasurfaces, Wang *et.al*[18,19] demonstrated terahertz QWPs with switchable single or multiple operation frequencies. Nakata *et al.*[20] demonstrated a switchable QWP operating at the specific frequency of 0.617 THz by designing a VO_2-based anisotropic checkerboard metasurface. Zhao *et al.*[21] proposed a switchable terahertz metamaterial that can be switched between an HWP and a QWP in the spectral band of 2.09-2.27 THz, corresponding to a relatively narrow bandwidth of 0.18 THz. Quite recently, some of the authors[22] proposed a metal-VO_2 metamaterial for achieving broadband switchable terahertz HWP/QWP, the bandwidth of which covers 0.66-1.40 THz, corresponding to a relative bandwidth of 71.8%. We further proposed a novel design philosophy making use of the transition from the overdamped to the underdamped resonance, and designed a VO_2 metal hybrid metasurface for achieving broadband dynamically switchable HWP/QWP in the spectral band of 0.8-1.2 THz[23].

Compared with liquid crystals and VO_2, graphene have many unique characteristics, including ultra-thin thickness (only 0.33 nm), low loss, and continuous and flexible tunability via electric biasing[24], chemical doping[25], or optical pumping[26]. Zhang *et al.*[27] and Tavakol *et al.*[28] respectively proposed switchable QWPs based on graphene metamaterials, and showed that the polarization state of the output wave can be dynamically switched among linear, left- and right-handed polarization by changing the graphene chemical potential. Zhang *et al.*[29] proposed functional switch from a QWP to an HWP within 4.80-5.10 THz based on a graphene metasurface. The corresponding bandwidth is only 0.3 THz and the relative bandwidth is only 6%. Guan *et al.*[30] propose a hybrid graphene-dielectric metasurface for realizing switchable HWP/QWP operating at the single frequency of 1 THz. Qi *et al.*[31] also proposed a graphene-based high-efficiency switchable HWP/QWP operating at the specific frequency of 15.96 THz. Quite recently, Zhang *et al.*[32] proposed a hybrid graphene-metal metasurface for achieving terahertz HWP/QWP in the frequency range of 1.38-1.72 THz. However, the corresponding bandwidth is 0.34 THz and the relative bandwidth is only 22%. Therefore, it remains challenging to design broadband switchable QWPs/HWPs based on graphene metasurfaces, greatly hindering their practical applications.

In this work, we propose a graphene-metal hybrid metasurface for achieving broadband switchable terahertz HWPs/QWPs. The metasurface unit cell is composed of a gold stripe and a graphene stripe on a thick gold film sandwiched by a dielectric spacer. We will show that the function of the proposed metasurface can be switched from a broadband HWP with polarization conversion ratio (*PCR*) exceeding 97% in the band of 0.7-1.3 THz, to a broadband QWP with ellipticity over 0.92 in the range of 0.78-1.33 THz. Therefore, these two switchable functionalities share the same spectral band of 0.78-1.3 THz, corresponding to a strikingly broad bandwidth of 0.52 THz and relative bandwidth of 50%, which is much larger than those of graphene-based metasurface HWPs/QWPs in the literatures[29-32].

2. Results and discussion

2.1. Simulation setup

Figure 1 illustrates the proposed metasurface acting as a broadband and dynamically switchable terahertz HWP/QWP. The metasurface unit cell consists of a gold short stripe and a graphene long stripe, which are perpendicular to each other and placed obliquely of 45° with respect to the *x*-axis. These graphene-gold hybrid stripes stand on a thick gold film sandwiched by a polyimide spacer, forming a metal-insulator-metal configuration. The metasurface can be fabricated using the state-of-the-art top-down microfabrication processes. A thick gold film is first deposited onto a silicon substrate, followed by spin-coating of a polyimide film of designed thickness. A monolayer graphene layer is then transferred on the top, and patterned into two-dimensional array of stripes using photolithography and reactive ion etching. Finally, the gold stripe array can be fabricated via photolithography, thermal evaporation, and liftoff processes[33].

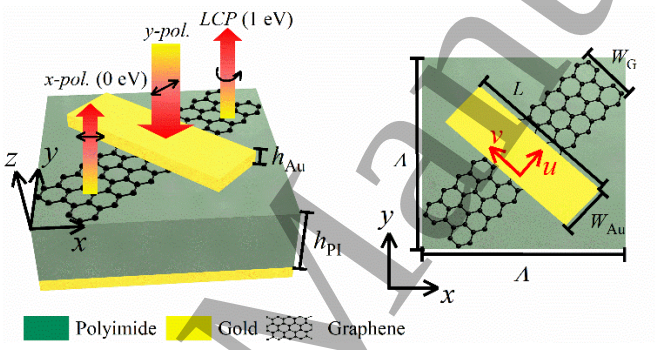

Fig. 1. (color online) Schematics of the proposed graphene-metal hybrid metasurface. (a) 3D view of the meta-surface, which can function as an HWP converting the incident linearly *y*-polarized terahertz wave into *x*-polarized wave when the Fermi level of graphene E_F is 0 eV, or as a QWP converting the incident *y*-polarized wave into right-handed circularly polarized wave when E_F = 1 eV. (b) Top view of the unit cell with Λ = 120 μm, W_{Au} = 30 μm, W_G = 20 μm, L = 90 μm, h_{PI} = 38 μm, and h_{Au} = 200 nm.

The operation principle of the proposed metasurface is as follows. When the Fermi level of graphene E_F is pinned at 0 eV, the graphene conductivity is as low as the dielectric material for the terahertz wave. In this scenario, the metasurface unit cell is effectively composed of the gold stripe, and thus the metasurface works as an HWP which can convert the incident linear polarization state into the orthogonal linear polarization state. When the graphene Fermi level is tuned to E_F =1 eV, which can be done via external stimulus, such as electric biasing[24] or optical pumping[26], the graphene conductivity is as high as metal-like material. In this case, the metasurface acts as a QWP that converts the linearly polarized incident wave into circularly polarized wave.

The polarization-dependent reflection amplitude and phase spectra of the proposed metasurface were numerically simulated using the frequency-domain solver in CST Microwave Studio. The unit cell boundary conditions were applied in the *x*

and y directions, and the open boundary condition was used in the z direction. Tetrahedral meshes with adaptive refinement process were applied. In all the simulations, gold was modelled using the lossy metal model with conductivity of 4.56×10^7 S/m, and the built-in material permittivity was adopted for polyimide.

The surface conductivity of graphene σ_G can be described by the Kubo equation with intraband and interband contributions[33], that is

$$\sigma_G = \sigma_{\text{intra}} + \sigma_{\text{inter}}. \quad (1)$$

According to Pauli exclusion principle, the interband contribution can be safely neglected compared with the intraband contribution for low terahertz frequencies at room temperature[34]. Thus the expression of the graphene conductivity can be simplified into[36]

$$\sigma_G \approx \sigma_{\text{intra}} = \frac{-ie^2 k_B T}{\pi\hbar^2(\omega+2i\tau)}\left[\frac{E_F}{k_B T} + 2\ln\left(e^{\frac{E_F}{k_B T}}+1\right)\right]. \quad (2)$$

Here e is the charge of an electron, k_B is the Boltzmann constant, T is the temperature, ω is the light frequency, τ is the carrier relaxation time from the impurities in graphene, and $\hbar$ is the Planck constant.

2.2. HWP function

Figures 2(a)(b) depict the simulated reflection amplitude and phase spectra of the proposed metasurface when the graphene Fermi level is set to be 0 eV, and under the incidence of u-v-polarized terahertz wave. Results show that $|r_{uu}|$ and $|r_{vv}|$ are almost equal to each other, and are close to 0.9 within the frequency range of 0.7-1.3 THz. Meanwhile, their phase differences are approximately equal to −180°, i.e., $\Delta\Phi = \Phi_{vv} - \Phi_{uu} = -180°$. Therefore, the graphene-metal hybrid metasurface with E_F = 0 eV can act as a broadband and efficient HWP.

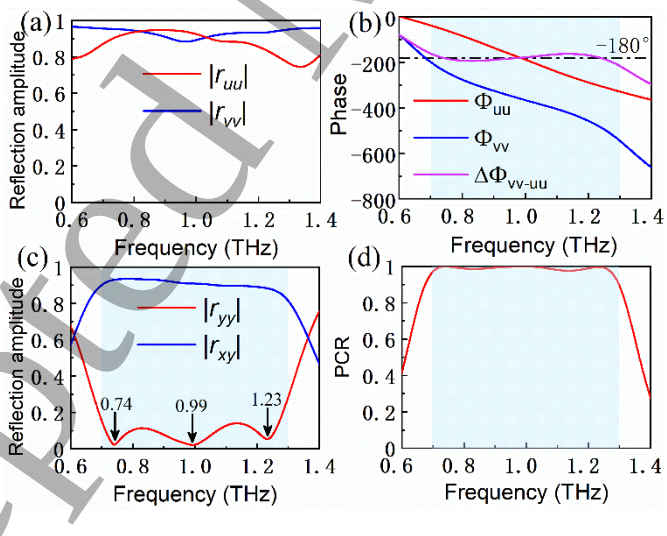

Fig. 2. (color online) Simulated reflection (a) amplitude $|r|$ (b) phase Φ spectra of the proposed hybrid metasurface with E_F = 0 eV under u- and v-polarized incidences. (c) Calculated reflection amplitude spectra for the co-polarization $|r_{yy}|$ and cross-polarization $|r_{xy}|$. (d) Calculated *PCR* spectra under y-polarized incidence. Blue regions in (b)-(d) indicate the broad operation band of the obtained HWP.

In order to evaluate the performance of the obtained HWP under the y-polarized incidence, we calculate the co-polarized and cross-polarized reflection amplitude

spectra, $|r_{yy}|$ and $|r_{xy}|$, and the spectra of the polarization conversion ratio (PCR), which can be calculated by

$$\mathrm{PCR} = |r_{xy}|^2/(|r_{xy}|^2 + |r_{yy}|^2). \quad (3)$$

Figure 2(c) shows that the cross-polarized reflection amplitude $|r_{xy}|$ is larger than 0.9, whereas the co-polarized reflection amplitude $|r_{yy}|$ is smaller than 0.1 in the range of 0.7-1.3 THz. For $|r_{yy}|$, there exist three dips locating at 0.74 THz, 0.99 THz and 1.23 THz. As a result, the calculated *PCR*s are larger than 0.97 within the broad spectral band of 0.7-1.3 THz. This corresponds to a relative bandwidth of $\Delta f/f_0 = 60\%$ with the central frequency locating at $f_0 = 1$ THz. These results suggest that the incident *y*-polarized terahertz wave can be efficiently converted to the *x*-polarized wave by the reflective metasurface with a broad operation bandwidth and high polarization conversion ratios. In other words, the proposed metasurface can work as a broadband and efficient HWP if the graphene Fermi level is 0 eV.

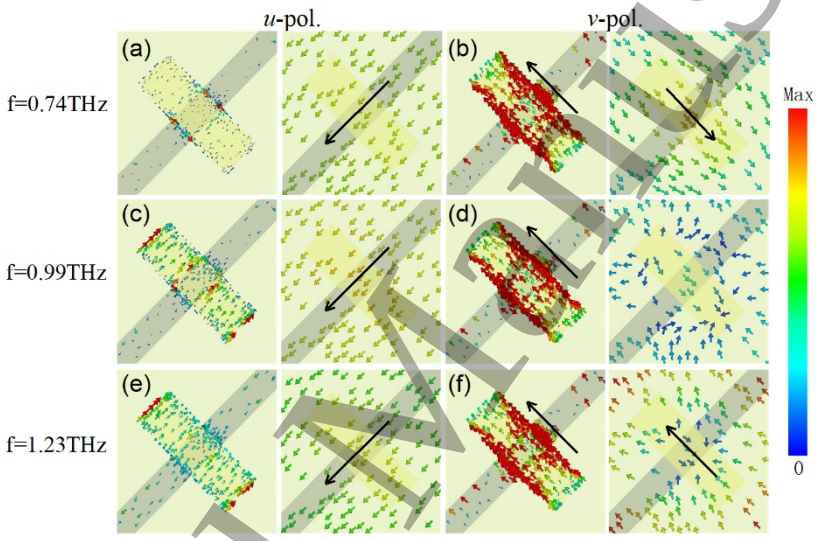

Fig. 3. (color online) Surface current distributions (arrows for directions and colors for strengths) on the gold and graphene stripes (1st and 3rd columns) and on the gold film (2nd and 4th columns) for three resonant frequencies of (a)(b) 0.74 THz, (c)(d) 0.99 THz, (e)(f) 1.23 THz when the graphene Fermi level is E_F = 0 eV. The 1st and 2nd columns are for the *u*-polarized incidence, and the 3rd and 4th columns are for the *v*-polarized incidence. The black arrows indicate the dominant current directions.

The broadband performance of the obtained HWP can be understood from the surface current distributions on the gold and graphene stripes and on the bottom gold film. Figure 3 depicts the surface current distributions under the *u*- and *v*-polarized incidences at the three resonant frequencies of $f = 0.74, 0.99,$ and 1.23 THz, for which $|r_{yy}|$ shows dips, as shown in Fig. 2(c). Figs. 3(a)(b) show that at 0.74 THz, the surface currents on the gold stripe are weak under the *u*-polarized incidence, but strong under the *v*-polarized incidence. These strong surface currents have opposite direction compared to those on the bottom gold film, producing a magnetic resonance under the *v*-polarized incidence. Similarly, at 0.99 THz and 1.23 THz, Figs. 3(c)(e) show that magnetic resonances are also generated under the u-polarized incidence, because the surface currents on the gold stripe have opposite direction to those on the

gold film. Fig. 3(d) shows that for the *v*-polarized incidence at 0.99 THz, the surface currents on the gold stripe are strong and have clear flow direction, whereas those on the gold film have counter-propagating directions and almost cancel each other. At 1.23 THz, the surface currents on the gold stripe and on the gold film are parallel to each other, resulting in an equivalent electric resonance, as shown by Fig. 3(f). Therefore, the broadband performance of the obtained HWP should originate from the superposition of these multiple resonances.

2.3. QWP function

We now tune the graphene Fermi level to E_F=1 eV. Fig.4(a) shows that the reflection amplitudes r_{uu} and r_{vv} are close to 0.9 for frequencies above 0.80 THz. Therefore, r_{yy} and r_{xy} are also close to each other, and their phase differences are approximate to –270° within the broadband frequency range of 0.78-1.33 THz, as shown in Figs. 4(b)(c). These results suggest that the proposed metasurface with E_F=1 eV now acts as a terahertz QWP.

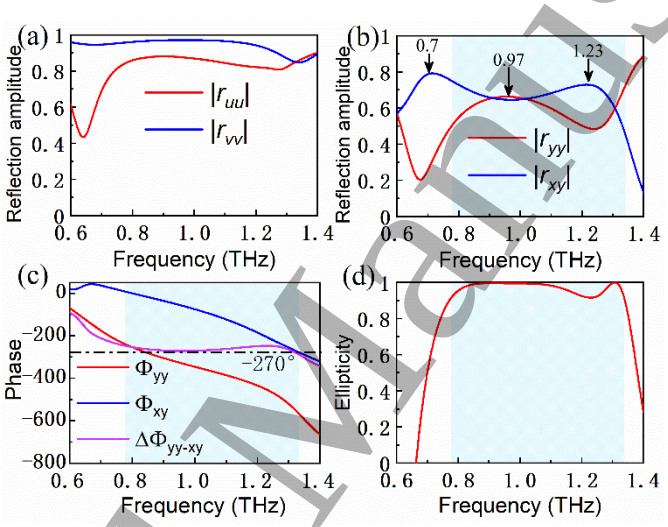

Fig. 4. (color online) Simulated reflection (a)(b) amplitude |*r*| and (c) phase spectra of the proposed hybrid metasurface with E_F = 1 eV. (d) The calculated ellipticity under linearly *y*-polarized incidence. Blue regions in (b)-(d) indicate the broad operation band of the obtained QWP.

The performance of the obtained QWP can be quantified using the ellipticity defined as $\chi \equiv S_3/S_0$, where the Stokes parameters S_0 and S_3 are expressed as[12]

$$S_0 = |r_{xy}|^2 + |r_{yy}|^2, \tag{4}$$

$$S_3 = 2|r_{xy}||r_{yy}|\sin(\Delta\Phi).$$

Here $\Delta\Phi = \Delta\Phi_{yy} - \Delta\Phi_{xy}$ means the phase difference between co-polarization and cross-polarization reflections. When χ equals to 1 or -1, the polarization state of the reflective terahertz wave is LCP or RCP, respectively. Fig. 4(d) shows that $\chi > 0.92$ over the broad frequency range of 0.78-1.33 THz. This result means that the graphene-metal hybrid metasurface with E_F=1 eV now functions as a broadband and efficient QWP that converts the incident linear *y* polarization into the RCP.

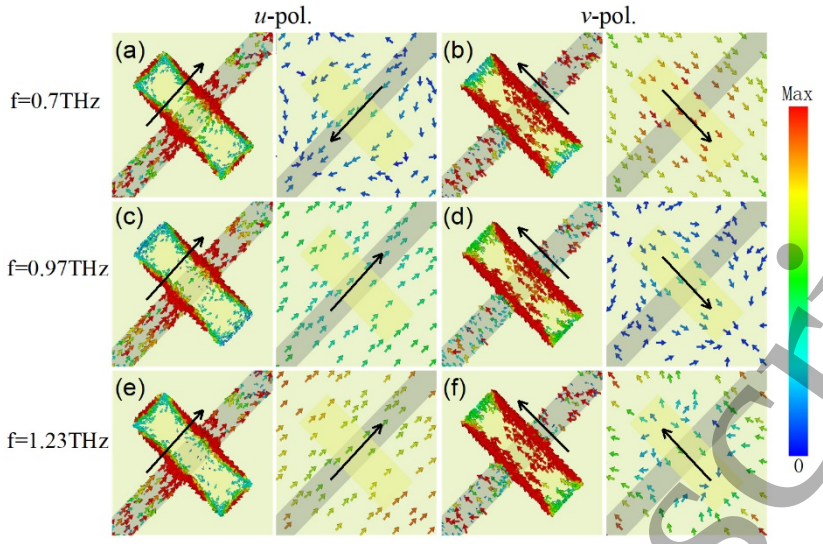

Fig. 5. (color online) Similar to Fig. 3 but for (a)(b) 0.7 THz, (c)(d) 0.97 THz, and (e)(f) 1.23 THz when E_F = 1 eV.

To understand the broadband performance of the obtained QWP, we also plot the surface current distributions on the gold and graphene stripes and on the bottom gold film. Here we use the three frequencies of 0.7 THz, 1.23 THz and 0.97 THz, which corresponds to two peaks and a dip in the $|r_{xy}|$ spectra, respectively, as shown by Fig. 4(b). Figs. 5(a)(b) show that at 0.7 THz, the surface currents on the gold and graphene stripes have the opposite direction compared with those on the gold film, forming magnetic resonances for both the *u*- and *v*-polarized incidences. For the *u*-polarized incidence at 0.97 THz, and for both the *u*- and *v*-polarized incidences at 1.23 THz, the surface currents the gold and graphene stripes and on the gold film have the same directions, resulting equivalent electric resonances, as shown by Figs. 5(c)(e)(f). For the v-polarized incidence at 0.97 THz, Fig. 5(d) shows that the surface currents on the gold and graphene stripes are strong and have well defined direction, whereas those on the gold film are weak and have counter-propagating directions. Therefore, the broadband performance of the obtained QWP should also originate from the superposition of multiple resonances.

2.4. Effects of key parameters

Figure 6 show the metasurface performances as the graphene Fermi level E_F varies continuously from 0 to 1.2 eV. The reflection amplitude keeps nearly unity for all graphene Fermi levels within 0.7 - 1.2 THz, which guarantees the high converting efficiency. Fig. 6(c) shows the absolute phase difference $|\Delta\Phi|$ depending on E_F. We note that there is a relatively homogenous region with gradual and continuous phase revolution, lying between about 0.7 and 1.1 THz. In this spectral region, the $|\Delta\Phi|$ evolves continuously from about 180° to 90° when E_F increases from 0 to 1 eV. In addition, as E_F further increases to 1.2 eV, $|\Delta\Phi|$ approaches 80°. Thus, our numerical results show a robust tolerance of the proposed metasurface.

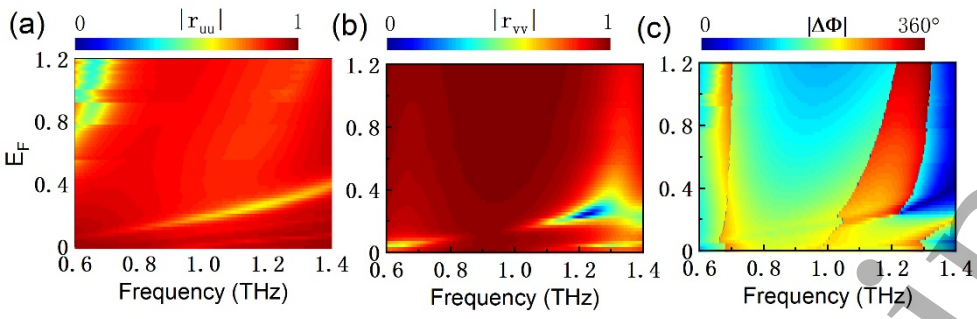

Fig. 6 (color online) (a) Reflection amplitude $|r_{uu}|$, (b) reflection amplitude $|r_{vv}|$ and (c) absolute phase difference $|\Delta\Phi|$ as graphene Fermi level varies 0 - 1.2 eV.

The influence of PI thickness h_{PI} is shown in Fig. 7. The reflection amplitude components $|r_{uu}|$ and $|r_{vv}|$ are almost unity for different h_{PI} from 34 to 42 μm and different graphene Fermi energies. In contrast, the absolute phase difference $|\Delta\Phi|$ exhibit distinct dependency on h_{PI} as shown in Fig. 7(c) and (f). For E_F = 0 eV, we note that the area of concerned frequency region (about 0.7–1.3 THz) in Fig. 7(c) could be divided into two subareas (about 0.7 - 1 THz and 1 - 1.3 THz), the former manifests that $|\Delta\Phi|$ increase while the latter manifests that $|\Delta\Phi|$ decrease as h_{PI} change from 34 to 42 μm. When h_{PI} equals 38 μm, the $|\Delta\Phi|$ is about 180° in both subareas (i.e., working as an HWP within 0.7 - 1.3 THz). For E_F = 1 eV, the absolute phase difference $|\Delta\Phi|$ changes gradually from about 76° to 97° as h_{PI} change from 34 to 42 μm. When h_{PI} equals 38 μm, the $|\Delta\Phi|$ is about 90° (i.e., working as a QWP within 0.78 - 1.33 THz).

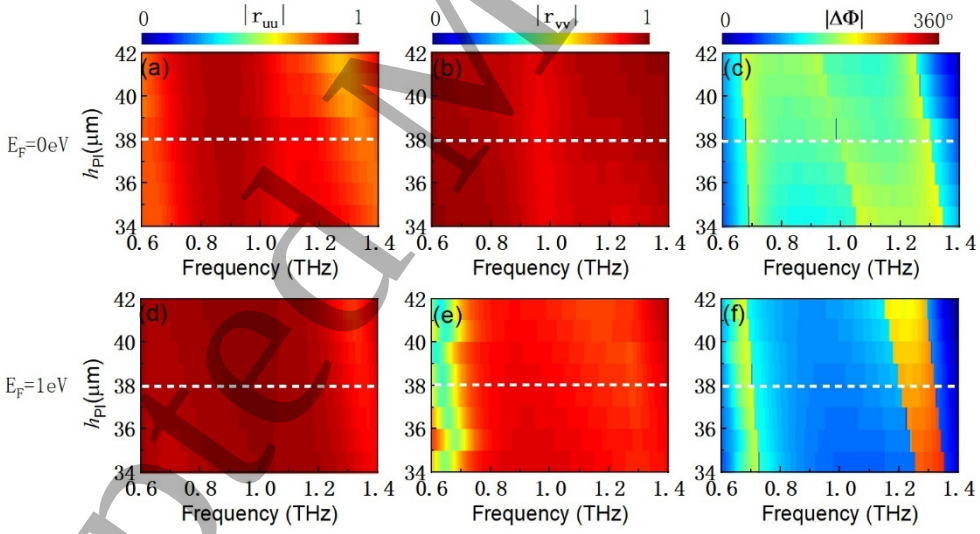

Fig. 7 (color online) Device performances dependent on thickness h_{PI}. (a)-(c) Reflection amplitude $|r_{uu}|$, $|r_{vv}|$, and absolute phase difference $|\Delta\Phi|$ when E_F = 0 eV, (d)-(f) Reflection amplitude $|r_{uu}|$, $|r_{vv}|$, and absolute phase difference $|\Delta\Phi|$ when E_F = 1 eV. The dashed white line indicates h_{PI} = 38 μm.

3. Conclusion

In conclusion, we have proposed a broadband switchable terahertz HWP/QWP based on a graphene-metal hybrid metasurface. Simulation results have shown that, by varying the Fermi energy of graphene from 0 eV to 1 eV, the function of the

reflective metasurface can be switched from an HWP, which converts the incident *y*-polarized terahertz wave into *x*-polarized wave, to a QWP that converts the *y*-polarized wave into right-handed circularly polarized wave. The polarization conversion ratio of the obtained HWP exceeds 97% over a wide band ranging from 0.7 THz to 1.3 THz, and the ellipticity of the obtained QWP is larger than 0.92 over 0.78-1.33 THz. Therefore, we have shown that the proposed metasurface can function either as an HWP or as a QWP in the spectral band of 0.78-1.3 THz. This corresponds to a strikingly broad bandwidth of 0.52 THz and relative bandwidth of 50%, which is much larger than the literature on graphene-based metasurface HWPs/QWPs. The broadband properties have been explained with the superposition of multiple resonances. We expect the designed broadband and dynamically switchable terahertz HWP/QWP will find applications in terahertz polarization-dependent systems of sensing, imaging, and telecommunications.

Acknowledgment

The scientific contributions from other people or groups are acknowledged here. Financial supports are given in the footnote on the first page.

References

1. Han Z and Bozhevolnyi S I 2013 Rep. Prog. Phys. **76** 016402
2. Hao J, Qiu M, and Zhou L 2010 Front. Phys. **5** 291
3. Chen H T, Taylor A J, and Yu N 2016 Rep. Prog. Phys. **79** 076401
4. Zhao J, Cheng Y, and Cheng Z 2018 IEEE Photon. J. **10** 4600210
5. Cheng Y, Fan J, Luo H, and Chen F 2019 IEEE Access **8** 7615
6. Fan J and Cheng Y 2020 J. Phys. D: Appl. Phys. **53** 025109
7. Chen L, Liao D, Guo X, Zhao J, Zhu Y and Zhuang S, 2019 Frontiers Inf. Technol. Electronic Eng. **20** 591
8. Cong L, Cao W, Tian Z, Gu J, Han J, and Zhang W 2012 New J. Phys. **14** 115013
9. Y.-J. Chiang and T.-J. Yen 2013 New J. Phys. **14** 115013
10. Grady N K, Heyes J E, Chowdhury D R, Zeng Y, Reiten M T, Azad A K, Taylor A J, Dalvit D A, and Chen H T 2013 Science **340** 1304
11. Cheng Y, Withayachumnankul W, and Upadhyay A 2014 Appl. Phys. Lett. **105** 181111
12. Cong L, Xu N, Gu J, Singh R, Han J, and Zhang W 2014 Laser Photonics Rev. **8** 626
13. Guo T and Argyropoulos C 2016 Opt. Lett. **41** 5592
14. Gao X, Yang W, Cao W, Chen M, Jiang Y, Yu X, and Li H 2017 Opt. Express **25** 23945
15. Ma S, Wang X, Luo W, Sun S, Zhang Y, He Q, and Zhou L 2017 EPL **117** 37007
16. Vasi´c B, Zografopoulos D. C, Isi´c G, Beccherelli R, and Gaji´c R 2017 Opt. Express **28** 124002
17. Ji Y-Y, Fan F, Wang X-H, and Chang S-J 2018 Opt. Express **26** 12852
18. Wang D, Zhang L, Gu Y, Mehmood M, Gong Y, Srivastava A, Jian L, Venkatesan T, Qiu C-W, and Hong M 2015 Sci. Rep. **5** 15020
19. Wang D, Zhang L, Gong Y, Jian L, Venkatesan T, Qiu C-W, and Hong M 2016 IEEE Photon. J. **8** 5500308 8
20. Nakata Y, Fukawa K, Nakanishi T, Urade Y, Okimura K, and Miyamaru F 2019 Phys. Rev. A

11 044008
21. Zhao J-X, Song J-L, Zhou Y, Liu Y-C, Zhou J-H 2020 Chin. Phys. Lett. **37** 64204
22. Luo J, Shi X, Luo X, Hu F, and Li G 2020 Opt. Express **28** 30861
23. Luo X, Hu F, and Li G 2021 J. Phys. D: Appl. Phys. **54** 505111
24. Fang Z, Thongrattanasiri S, Schlather A, Liu Z, Ma L, Wang Y, Ajayan P M, Nordlander P, Halas N J, and Garc´ıa de Abajo F J 2013 ACS Nano **7** 2388
25. Liu H, Liu Y, and Zhu D B 2011 J. Mater. Chem. **21** 3335
26. Ryzhii V. and Ryzhii M 2007 J. Appl. Phys. **101** 083114
27. Zhang Y, Feng Y, Zhu B, Zhao J, and Jiang T 2015 Opt. Express **23** 27230
28. Tavakol M. R, Rahmani B, and Khavasi A 2019 IEEE Photon. Technol. Lett. **31** 931
29. Zhang W, Jiang J, Yuan J, Liang S, Qian J, Shu J, and Jiang L 2018 OSA Continuum **1** 124
30. Guan S, Cheng J, Chen T, and Chang S 2019 Opt. Lett. **44** 5683
31. Qi X, Zou J, Li C, Zhang J, C. Guo C, and Zhu Z 2020 Opt. Express **28** 39430
32. Zhang J, Zhang K, Cao A, Liu Y, and Kong W. 2020 Opt. Express **28** 26102
33. Tamagnone M, Capdevila S, Lombardo A, Wu J, Centeno A, Zurutuza A, Ionescu A, Ferrari A and Mosig J, 2018 arXiv:1806.02202
34. Tao J, Yu X, Hu B, Dubrovkin A, and Wang Q J 2014 Opt. Lett. **39** 271
35. Falkovsky L and Pershoguba S 2007 Phys. Rev. B 76 153410
36. Ju L, Geng B, Horng J, Girit C, Martin M, Hao Z, Bechtel H, Liang X, Zettl A, and Shen Y 2011 Nat. Nanotechnol. 6 630